Topography Driven Spreading

G. McHale,* N. J. Shirtcliffe, S. Aqil, C. C. Perry, and M. I. Newton
School of Biomedical and Natural Sciences, The Nottingham Trent University, Clifton Lane, Nottingham NG11 8NS, United Kingdom
(Received 14 December 2003; published 15 July 2004)

Roughening a hydrophobic surface enhances its nonwetting properties into superhydrophobicity. For liquids other than water, roughness can induce a complete rollup of a droplet. However, topographic effects can also enhance partial wetting by a given liquid into complete wetting to create superwetting. In this work, a model system of spreading droplets of a nonvolatile liquid on surfaces having lithographically produced pillars is used to show that superwetting also modifies the dynamics of spreading. The edge speed-dynamic contact angle relation is shown to obey a simple power law, and such power laws are shown to apply to naturally occurring surfaces.

DOI: 10.1103/PhysRevLett.93.036102 PACS numbers: 68.08.Bc, 68.03.Cd

Liquids and droplets of liquids are of great importance in many processes ranging from ink-jet printing to DNA technologies. Understanding how droplets sit on solid surfaces and how they spread out to form films is relevant to problems as diverse as ring-stain formation due to the drying of spilled drops of coffee [1] to microfluidics [2]. However, solid surfaces are rarely smooth and flat, but are usually rough or have undulations, pores, or other surface structure. In recent years, the effect of surface topography on wetting has become the focus of much interest since the demonstration in 1996 by Onda *et al.* [3] of a hydrophobic fractal-like surface. Since then, these superhydrophobic surfaces have been constructed in a wide variety of ways, from lithographic fabrication [4] to transformation of simple plastics [5]. Superhydrophobic surfaces have a range of interesting properties from droplet impact with a time of contact independent of speed [6] to drops rolling down these surfaces under capillary forces at a speed faster than a solid sphere would roll under gravity [7]. In nature, some plants, such as *Nelumbo nucifera* (L.) *Druce,* structure the surface of their leaves so that their chemical hydrophobicity is enhanced into superhydrophobicity [8] and, in the Namibian desert, a beetle, *Stencora sp.,* controls the topography of its back surface together with regions of chemical hydrophobicity and hydrophilicity to collect drinking water from fog-laden wind [9]. Superhydrophobic principles also apply to other liquids whose equilibrium contact angles can also be enhanced by surface roughness or texture. While the topographic enhancement of contact angles to create nonwetting surfaces has been extensively studied, the opposite effect of topography induced reduction in droplet contact angles and increases in the rate of droplet spreading to create superwetting and superspreading effects has not been so extensively studied.

For a droplet, hydrophobicity and wetting is governed by the balance of forces at the contact line arising from the three interfacial tensions, γ_{SV}, γ_{SL}, and γ_{LV}, occurring at the solid-vapor, solid-liquid, and liquid-vapor interfaces, respectively. Projecting the liquid-vapor force horizontally using the contact angle θ and establishing a horizontal force balance gives Young's law:

$$\cos\theta_e^s = \frac{\gamma_{SV} - \gamma_{SL}}{\gamma_{LV}}, \tag{1}$$

where θ_e^s is the equilibrium contact angle. An alternative view to balancing forces is to consider the interfacial tensions as surface energies per unit area of the interface. In this approach the effect of increasing the area covered by the contact line by a small amount, ΔA, is to replace the solid-vapor interface by a solid-liquid interface and so change the surface free energy by $(\gamma_{SL} - \gamma_{SV})\Delta A$. In addition, the movement of the liquid creates an additional liquid surface area of $\Delta A\cos\theta$, resulting in a surface free energy increase of $\gamma_{LV}\Delta A\cos\theta$ [10]. If the surface free energy is to be at a minimum, then the overall change in surface free energy must vanish and this gives Young's law for the equilibrium contact angle [Eq. (1)]. Roughness, or topographic structuring, of the surface modifies this argument because the solid surface has a larger area $r\Delta A$ than the horizontal projection of the area, where r is a roughness factor and is greater than 1. While the roughness alters the surface free energy change at the solid interface, it does not alter the liquid-vapor contribution. In energetic terms, the overall effect of topography is to result in an equilibrium contact angle on a rough surface, θ_e^r, given by Wenzel's equation [11]:

$$\cos\theta_e^r = r\cos\theta_e^s. \tag{2}$$

Wenzel's equation predicts that roughness will emphasize the intrinsic wetting behavior of a surface as determined by its surface chemistry. Enhancement of both nonwetting and complete wetting are predicted. If the contact angle on the smooth surface is larger than 90°, roughness will further increase the observed contact angle, but if it is less than 90°, roughness will reduce the observed contact angle. The changes in hydrophobicity induced by roughness can be large with equilibrium

contact angles of ~115° on flat surfaces being converted to angles in excess of 165° on rough surfaces. Moreover, Wenzel's equation suggests that, on a rough surface, complete wetting will be achieved for all partial wetting liquids satisfying $\cos\theta_e^s > 1/r$.

In practice, superhydrophobic surfaces do not entirely follow Wenzel's equation but involve incomplete liquid penetration so that the droplet sits on a composite air-solid surface; the contact angle on a smooth surface for which roughness results in nonwetting behavior is then reduced below 90° [12]. In this form of superhydrophobicity (or, if the liquid is not water, super-non-wetting), the equilibrium contact angle is determined by the fraction of area of the solid tops, φ_s, in the planar projection of the area rather than the roughness r. The equilibrium contact angle is then given by the Cassie-Baxter equation [13,14]

$$\cos\theta_e^r = -\varepsilon + \varphi_s(\cos\theta_e^s + \varepsilon), \tag{3}$$

where $\varepsilon = 1$. In a similar manner, it can be anticipated that the complete wetting predicted by Wenzel's equation will occur only if the surface texture can completely imbibe the volume of the deposited droplet. If it cannot, then an equilibrium droplet may form on a composite liquid-solid surface, and a Cassie-Baxter type of equation, Eq. (3) but with $\varepsilon = -1$, will likely be valid [15].

In this work we show that similar considerations leading to modification of equilibrium angles can be applied to the dynamics of liquids spreading on rough or textured surfaces. When a droplet spreads on a smooth and flat surface, a Poiseuille flow occurs and a viscous dissipation proportional to $\eta\nu_E^2/\theta$ is created, where η is the viscosity and ν_E is the edge speed of the drop [10]. This dissipation is equal to $F\nu_E$, where the driving force F is proportional to the unbalanced component of the liquid-vapor surface tension: $\gamma_{\mathrm{LV}}(\cos\theta_e^s - \cos\theta)$. For small angles and complete wetting surfaces ($\theta_e^s = 0°$), this gives the Hoffman–de Gennes law with the edge speed proportional to the cube of the dynamic contact angle, i.e., $\nu_E \propto \theta^3$. Roughness will modify the driving force to $\gamma_{\mathrm{LV}}(r\cos\theta_e^s - \cos\theta)$ and with the viscous dissipation we predict that for small angles an additional term directly proportional to the dynamic contact angle occurs [16], i.e.,

$$\nu_E \propto \theta(r-1) + \theta(\theta^2 - r\theta_e^{s2})/2. \tag{4}$$

The derivation leading to this equation ignores any topography induced modification to the logarithmic cutoff term occurring in the viscous dissipation [10]. It is also known that a prewetting film can spread ahead of the macroscopic droplet and the thickness of this film, whether the drop effectively spreads on a composite solid-liquid surface and the effect of any slippage have not been included. Nonetheless, Eq. (4) provides a first approximation of how dynamic wetting may be modified by surface topography. For complete wetting ($\theta_e^s = 0°$), the effect of roughness is predicted to produce a transition from a cubic law to a linear law [16] and the spreading of the droplet to become determined by the topography. We emphasize here that the topography changes the surface free energies involved in droplet spreading and so the predicted effects are not simply about a film of liquid spreading within the channels defined by the topography.

To test the prediction for topography induced superwetting, we created multiple sets of surfaces structured with circular pillars of diameter 15 μm arranged in a square lattice with a 30 μm lattice parameter across an area of size 1 cm × 1 cm. The heights of the pillars were increased systematically until a maximum height of 70 μm, equal to an aspect ratio greater than 4, was achieved; above this height maintaining vertical side walls for the pillars became difficult. These surfaces were fabricated by patterning a layer of SU-8 photoresist (Fig. 1). Equilibrium measurements for drops of water gave contact angles of 84° on the flat SU-8 and 144° on the tallest of the patterned surfaces compared to a predicted 146° from Eq. (3); when hydrophobized these angles were 115°, 155°, and 155°, respectively. We therefore conclude that these surfaces demonstrate superhydrophobic properties of the Cassie-Baxter type [Eq. (3)]. We also investigated the wetting and nonwetting properties of these surfaces for a range of liquids by measuring the equilibrium contact angles using small droplets whose volume (~ 1 μl) could be entirely accommodated within the texture of the surfaces. We observed complete wetting (i.e., film formation) on tall SU-8 pillar surfaces for liquids, such as ethylene glycol, which have contact angles as high as 51° on the flat SU-8 surface [17]. From this we conclude that a Wenzel-type enhancement of complete wetting can occur on these surfaces.

The experiments on dynamic wetting used video profiles of the spreading of small droplets (initial volume ~1 μl) of nonvolatile PDMS (polydimethylsiloxane) oils of viscosity 10 000 cSt; PDMS completely wets the flat

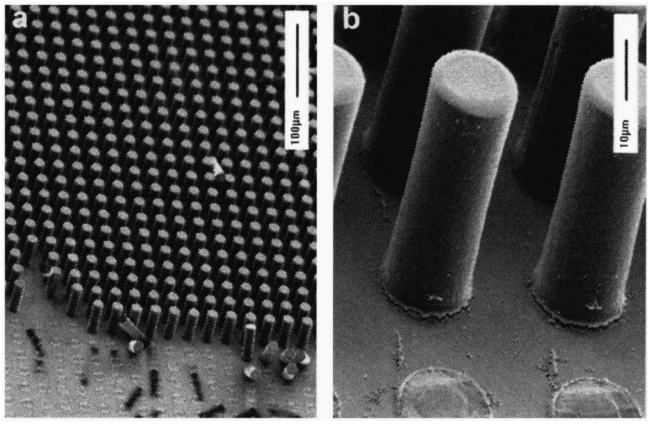

FIG. 1. Scanning electron microscope images of lithographically structured surfaces showing a square lattice of 15 μm diameter cylindrical pillars with a 30 μm lattice parameter: (a) view of a field of pillars and (b) close-up view of the pillars.

SU-8 surface. The size of these droplets was less than the capillary length so that surface tension dominates and the shape of the droplet is a spherical cap. From the side-profile images of the drop, we determined the volume, contact diameter, and dynamic contact angle and confirmed the validity of the spherical cap shape assumption. The drop volume remained constant over much of the spreading time, but the final stage in the spreading was characterized by the PDMS draining into and filling the surface structure. Visually, the separation between the droplet spreading regime and draining into a film was clear for the surfaces with the tallest patterns. On these patterns the surface structure can be seen in the images, via the surface reflected light, during the period the droplet spreads from initial contact angles in excess of 70° down to around 30–35°. As the latter angles occur, the reflected view of the structure of the surface is lost in the image as a film completely fills the pattern at the droplet edge and spreads out in advance of the droplet. During this final stage, the drop dynamics changed due to the loss of drop volume and the complication of the drop spreading on a prewetting film of the oil. The speed of the droplet spreading for drops of similar volume was visibly faster on the textured surfaces than on the flat surfaces. Previous studies of spreading of droplets of PDMS on smooth and abraded glass surfaces have been reported by Cazabat and Cohen-Stuart [18], but these studies mainly involved data for low contact angles and the film spreading stage. In their work, contact area was measured rather than drop profile. The technique used to produce the abraded surfaces would also have resulted in a constant roughness factor, whereas in our case the roughness factor is varied systematically in a highly controlled manner.

When the volume of a spreading droplet is constant, the edge speed can be converted into a rate of change of the angle. For a spherical cap shaped droplet, the edge speed-dynamic contact angle relation for a rough or textured surface becomes

$$\frac{d\theta}{dt} \propto -\theta^{7/3}[(r-1) + (\theta^2 - r\theta_e^{s2})/2]. \qquad (5)$$

For a smooth ($r = 1$) and complete wetting surface ($\theta_e^s = 0°$), this equation integrates to give a simple (Tanner's) power-law behavior, $\theta \propto (t + t_0)^{-n}$ with $n = 3/10$ for the dynamic contact angle [10,16]. If the surface roughness dominates, a simple power-law behavior should still be observed, but with an exponent of $n = 3/4$. In the intermediate regime the exponent n will lie between these two values. Similarly, the edge speed-dynamic contact angle relation [Eq. (4)] will appear to follow a power law $\nu_E \propto \theta^p$ with the exponents related by $n = 3/(3p + 1)$. Equation (5) also predicts that, for sufficiently high values of r, liquids which are partially wetting on a smooth surface, but complete wetting on the rough surface, may also follow a power law with $n = 3/4$.

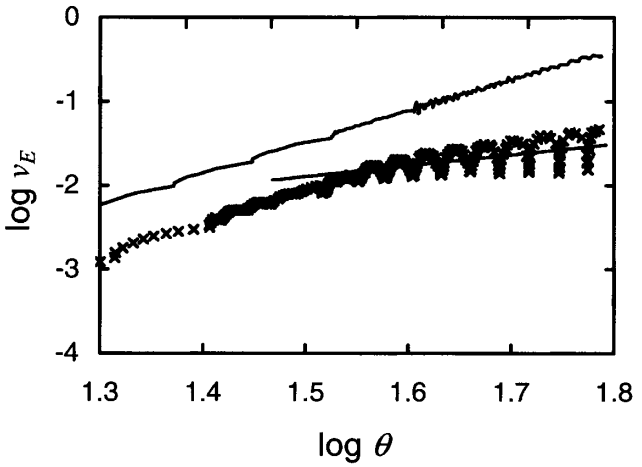

FIG. 2. A log-lot plot of the edge speed-dynamic contact angle relationship for a polydimethylsiloxane droplet on a surface with 15 μm diameter pillars of height 45 μm and lattice parameter 30 μm (×); the slope of these data during the initial spreading ($p = 1.296$) is also shown. The upper solid curve with a slope of $p = 3$ is data for a smooth surface (shifted upwards by 0.5 for clarity).

A typical log-log plot of the edge speed (determined numerically from the contact diameter) and dynamic contact angle is shown in Fig. 2; the solid line indicates the initial trend of the slope p. Data equivalent to Fig. 2 were obtained a minimum of 6 times for each height pattern and repeated on several separately fabricated surfaces of the same height pattern. Figure 3 shows the log-log plot of the dynamic contact angle data, corresponding to the data in Fig. 2, and its fit to $\theta = A/(t + t_0)^n$; the percentage change in volume with time is also given and shows that the fit no longer follows the data once the volume loss exceeds ~1% of the initial drop volume. Analysis of the oscillations in the edge speed

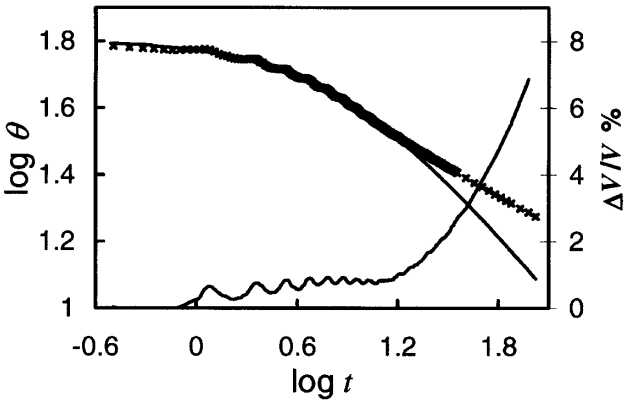

FIG. 3. A log-log plot of the dynamic contact angle and time with a fit of $\theta \propto 1/(t + t_0)^{0.614}$ for the experiment on the textured surface corresponding to the data in Fig. 2. The percentage change in drop volume is also shown (lower curve and right-hand axis).

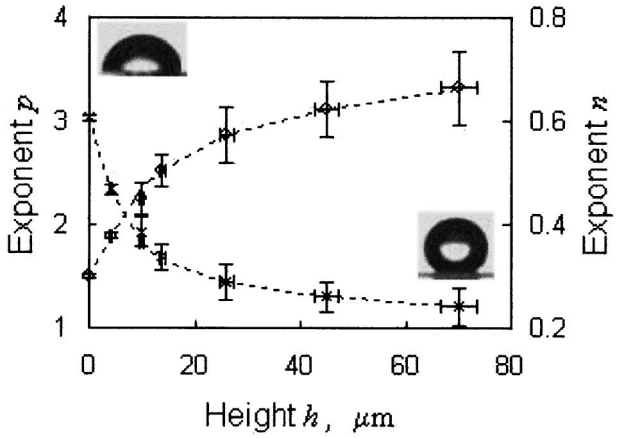

FIG. 4. Exponents p extracted from the edge speed-dynamic contact angle data ($\times$) for spreading of polydimethylsiloxane oils on textured surfaces; the dotted curve indicates the trend from cubic to linear form with increasing pillar height. Each data point is an average of experiments on several drops and surfaces. The dynamic contact angle-time exponent n variation with pillar height ($\bigcirc$) is indicated by the right-hand axis. The inset images show the equilibrium shape of water droplets on the flat surface ($\theta_e = 84°$) and a surface consisting of 52 μm tall pillars ($\theta_e = 142°$).

indicates that successive maxima and minima correspond to changes in contact diameter of the drop equal to the lattice parameter (i.e., 30 μm); this is due to microscopic stick-slip motion of the droplet edge reflecting the lattice of the pillars.

Figure 4 summarizes the complete data set for the spreading exponents of PDMS oils on the multiple surfaces. The data points for the exponent, p ($\times$ symbols and left-hand axis), show that as the height of the pillars increases the power law changes from $p = 3$ towards $p = 1$ as predicted in Eq. (4). Exponents p determined using the edge speed-contact angle method are slightly lower than those determined using fits to the dynamic contact angle variation with time, but in both cases the trend from cubic to linear is unambiguous. The dynamic contact angle-time exponent n variation with pillar height [($\bigcirc$) indicated by the right-hand axis] shows a change from Tanner's law $n = 3/10$ towards $n = 3/4$ as predicted by Eq. (5). The insets in Fig. 4 show the equilibrium shapes of drops of water on flat and tall patterned surfaces and illustrate that, as increasing pattern height causes equilibrium nonwetting of water, it can also result in faster spreading dynamics for droplets of other liquids. In a final set of experiments, we investigated whether a naturally occurring superhydrophobic surface would also, when presented with a complete wetting liquid, demonstrate dynamic contact angle behavior consistent with Eq. (4). PDMS oil drops spreading on a sprout leaf (*brassica oleracea*), which has an equilibrium contact angle to water in excess of 165°, resulted in exponents $p \sim 2$, thus indicating topography driven spreading.

Our measurements support the idea that a superhydrophobic surface can also act as a superwetting surface. Moreover, complete wetting liquids spread on these surfaces at a greater speed than on flat surfaces and their dynamics follow a simple power-law behavior. This modification of complete wetting and spreading has significance for processes such as inking, where enhanced spreading is desired, and in coating processes where the maximum coating speed is determined by the dynamic contact angle reaching 180°. In addition, current attempts to create superhydrophobic self-cleaning surfaces (e.g., for use in automobile windows) may suffer as a result of the surface roughness/structuring causing difficulty in removing films of oil. Finally, in nature the surface topography used by some plants (and beetles) to achieve water-repellent and self-cleaning surfaces may lead to a greater susceptibility to man-made environmental contamination.

The authors acknowledge the financial support of the UK EPSRC and MOD/Dstl.

*To whom correspondence should be addressed.
Electronic address: glen.mchale@ntu.ac.uk

[1] R. D. Deegan, O. Bakajin, T. F. Dupont, G. Huber, S. R. Nagel, and T. A. Witten, Nature (London) **389**, 827 (1997).
[2] M. W. J. Prins, W. J. J. Welters, and J. W. Weekamp, Science **291**, 277 (2001).
[3] T. Onda, S. Shibuichi, N. Satoh, and K. Tsujii, Langmuir **12**, 2125 (1996).
[4] D. Öner and T. McCarthy, Langmuir **16**, 7777 (2000).
[5] H. Y. Erbil, A. L. Demirel, Y. Avci, and O. Mert, Science **299**, 1377 (2003).
[6] D. Richard, C. Clanet, and D. Quéré, Nature (London) **417**, 811 (2002).
[7] D. Richard and D. Quéré, Europhys. Lett. **48**, 286 (1999).
[8] C. Neinhuis and W. Barthlott, Ann. Bot. (London) **79**, 667 (1997).
[9] A. R. Parker and C. R. Lawrence, Nature (London) **414**, 33 (2001).
[10] P. G. De Gennes, Rev. Mod. Phys. **57**, 827 (1985).
[11] R. N. Wenzel, Ind. Eng. Chem. **28**, 988 (1936).
[12] J. Bico, C. Tordeux, and D. Quéré, Europhys. Lett. **55**, 214 (2001).
[13] R. E. Johnson and R. H. Dettre, Adv. Chem. Ser. **43**, 112 (1964).
[14] D. Quéré, A. Lafuma, and J. Bico, Nanotechnology **14**, 1109 (2003).
[15] D. Quéré, Physica (Amsterdam) **313A**, 32 (2002).
[16] G. McHale and M. I. Newton, Colloids Surf. A **206**, 193 (2002).
[17] G. McHale, N. J. Shirtcliffe, and M. I. Newton, Analyst (Cambridge, UK) **129**, 284 (2004).
[18] A. M. Cazabat and M. A. Cohen-Stuart, J. Phys. Chem. **90**, 5845 (1986).